Fabrication of Free-Standing Porous $BaTiO_3$ Thick Films by Indirect Selective Laser Sintering

F.B. Mendes, L.C. Ferreira, R.B. Oliveira and M.R.B. Andreeta*

Department of Materials Engineering, Federal University of São Carlos, Washington Luís Road SP 310, km 235, São Carlos, São Paulo 13565-905, Brazil

Abstract: The fabrication of free-standing porous thick films of ferroelectric $BaTiO_3$, using a laser-assisted technique, is presented as a novel alternative to conventional methods. This approach adapts Indirect Selective Laser Sintering (ISLS) to create green films in a single laser pass, avoiding the complexities of traditional processes. Using commercial $BaTiO_3$ powder and polyamide 12 as raw materials, laser processing parameters such as scanning laser speed and power were optimized to produce green $BaTiO_3$ thick films with different thicknesses. After laser processing, the films were conventionally sintered and characterized for phase composition, microstructure, porosity, and electrical properties. X-ray diffraction and Raman spectroscopy confirmed the tetragonal $BaTiO_3$ phase, while mercury intrusion porosimetry revealed a bimodal pore distribution. Impedance spectroscopy demonstrated a positive temperature coefficient of resistivity (PTCR) effect, with a peak resistivity near the Curie temperature. The PTCR behavior is hypothesized to arise from better oxygen adsorption due to the porosity and oxygen vacancies generated during sintering by carbon residues from polyamide degradation. The results demonstrate that ISLS is a versatile technique for producing high-quality, free-standing porous ceramic thick films with potential for a wide range of applications.

Keywords: Selective Laser Sintering, Free-Standing, Thick Films, $BaTiO_3$, CO_2 Laser; Resistivity; Polyamide.

1. INTRODUCTION

The production of thick films can be traced back to ancient Greek and Egyptian civilizations, where metal sheets were utilized as ornamental materials [1]. However, it was only in the 19th century that researchers, such as Michael Faraday [2], got interested in the optical and electrical behavior of thin and thick films and how their properties differ depending on their thickness. Interestingly, some of those first thick films were free-standing, which is again attracting interest in technological applications [3-5].

Free-standing thick films are notable for two primary reasons. The first one is related to the production process. The absence of substrate mitigates possible chemical reactions and contamination of the film, eliminates constraints related to the melting point or degradation imposed by the substrate compound, and also avoids any possible expansion mismatch [3]. The second reason concerns their intrinsic properties. The absence of substrate, for example, does not limit the electromagnetic spectrum absorptions/transmission and the vibrational modes remain unaffected, as well as their electrical and magnetic properties [5].

The fabrication process of free-standing thick films for ferroelectric compounds is typically achieved through methods such as tape casting, aerosol deposition, or sacrificial layer-based screen-printing techniques [3, 5, 6]. These methods serve as forming techniques to achieve the desired thick film geometry. Although efficient, they often require a complex and long preparation process, with multiple steps to create the thick film, before the high-temperature annealing/sintering. Furthermore, the usual goal of the traditional free-standing thick film preparation techniques is to produce a dense thick film. However, for some applications, the presence of pores is desired to improve the properties of the compound, such as in the case of $BaTiO_3$. Porous $BaTiO_3$ ceramics have proven to be advantageous for PTCR device applications. It is assumed that the presence of pores facilitates oxygen adsorption at the grain boundaries, increasing their potential barrier [7]. The techniques typically used to create porosity in $BaTiO_3$ ceramics are based on *in situ* volatilization of compounds during the sintering process, such as the thermal decomposition of barium titanyl oxalate, $BaTiO(C_2O_4)_2 \cdot 4H_2O$, graphite, borides, silicides, and carbide powders [8].

The production of porous, free-standing thick films of ferroelectric compounds can be simplified by using high-power lasers in the forming process. Regarding material processing, lasers are often utilized as a highly controllable and localized source of thermal energy. A well-established material processing technique involving lasers is the Selective Laser Sintering (SLS) [9], whose applications were initially focused on polymeric and metallic materials. The relatively limited research on ceramics can be attributed to challenges in

*Address correspondence to this author at the Federal University of São Carlos (UFSCar) Materials Engineering Department (DEMa) 13565-905 São Carlos-SP, Brazil; E-mail: andreeta@ufscar.br

E-ISSN: 2410-4701/24

processing these materials, including high melting points, low thermal shock resistance, reduced plasticity, and low laser absorption. To address these issues, Indirect Selective Laser Sintering (ISLS) was developed as an alternative approach for fabricating ceramic components [9].

In ISLS, an organic polymer serves as a binding phase. During laser irradiation, the polymer melts, binding the ceramic particles. This method facilitates the production of crack-free parts, but the green and final densities are typically low (<60%). The properties of the green and final bodies depend on the morphology and composition of the powder, as well as the ISLS processing parameters and subsequent post-processing operations. The low-density ceramics prepared by ISLS are usually considered a drawback of the technique since many studies on this subject are searching for new and complex geometries for structural ceramics applications [9].

This work presents the viability study for a laser-assisted fast, free-standing thick film-forming process, which is based on an adapted ISLS technique. Using this approach, it was possible to produce porous, green free-standing films with thickness in the interval between hundreds of microns up to millimeters, using a single pass of the laser, without any additional powder deposition. After the conventional sintering process, the films were characterized by X-ray diffraction, Raman spectroscopy, impedance spectroscopy, and mercury intrusion porosimetry.

2. MATERIALS AND METHODS

2.1. Starting Materials

The raw materials used were commercial $BaTiO_3$ (Sigma Aldrich, 99%) and polyamide 12 (DuraForm - SLS) powders in a 60/40 weight ratio. After the drying process to remove water adsorption, the powdered reagents were weighed on an analytical balance to achieve the desired proportion. The raw materials were manually mixed and subsequently sealed in a cylindrical plastic container, then placed in a rotary mixer (Speed-mixer Flaktek DAC 1200-500). A 4-minute cycle at a rotational speed of 1200 rpm was performed to ensure powder homogeneity. The mixture was then transferred to a Petri dish with a diameter of 75 mm and a height of 13 mm, filling it to form the powder bed. No mechanical pressure was applied to the powder bed, and the surface was kept as smooth as possible.

2.2. Laser Processing

The surface heat treatment was performed using a CO_2 laser (Synrad, Evolution model) controlled by a conventional galvanometric component with an X-Y coordinate irradiation system for the sample. This process resulted in the production of a well-defined line on the surface of the powder bed, which was scanned at varying speeds and laser power across the powder bed surface. The laser beam incident on the surface of the powder bed generated a temperature gradient in the irradiated region. The beam was displaced along the perpendicular direction with respect to the scanned line created, forming the free-standing porous film through a single pass of the laser beam over the powder bed surface. At the end of the treatment, the green film was allowed to cool to room temperature and removed from the powder bed with a spatula. A schematic diagram of the laser process is shown in Figure **1** [8, 10].

2.1. Conventional Sintering

The $BaTiO_3$/PA films were sintered in alumina crucibles in an electric furnace (Furnace CM Inc. Bloomfield N.J.). The crucibles were covered with unsealed alumina plates to minimize temperature fluctuations and thermal gradients. The heating process consisted of two steps. In the first one, the temperature was increased at a rate of 3°C/minute and then held at 500°C for 2 hours to remove the polyamide, followed by second step with temperature increase at the same rate and held at 1200°C for 3 hours to complete sintering, before returning to room temperature at a rate of 10°C/minute.

2.2. Characterization

The crystal structure of the films after conventional sintering was analyzed through Raman spectroscopy (Raman-HR-TEC-785, Stellarnet, with an excitation wavelength of 785 nm) and X-ray diffraction using a micro-area accessory (Rigaku - Ultima IV goniometer). The X-ray diffraction measurement was conducted at a scanning rate of 1°/min within a (2θ) angle ranging from 20° to 80°. Phase identification was performed with the assistance of the PDXL2 software (Rigaku). The particle morphology was analyzed using a bench scanning electron microscopy (JCM7000 – Jeol). Samples were attached to a support using double-sided carbon tape. To make the samples electrically conductive, they were coated with a thin gold layer via sputtering deposition. The porosity and pore size of the

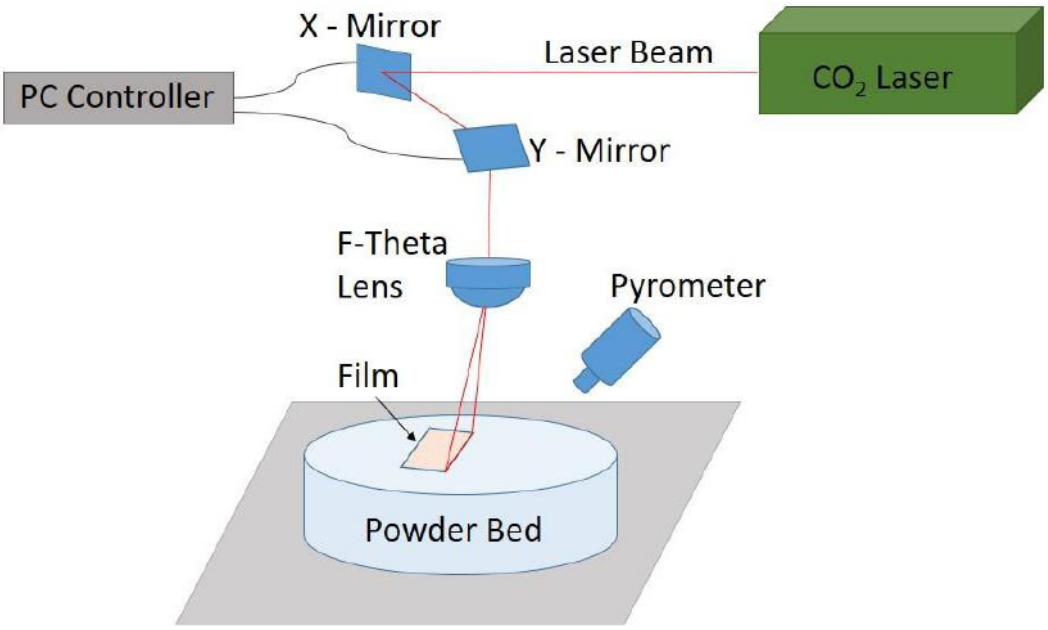

Figure 1: Schematic representation of the adapted Indirect Selective Laser Sintering (ISLS) used to fabricate the green $BaTiO_3$ thick films [10].

films were measured using the mercury intrusion porosimetry - MIP (Aminco Winslow porosimeter, model no. 5-7118). Electrical characterization was performed through solid-state impedance spectroscopy (Novocontrol Alpha-A High-Frequency analyzer). The measurements were carried out in air, at temperatures ranging from 25 to 300 °C, taken every 10 °C, after waiting for the thermal stabilization of the apparatus. The frequency range of 10^7 to 1 Hz, applying a voltage of 100 mV (AC). The sample preparation was made first by polishing the surfaces with sandpaper, followed by a gold electrode deposition layer on both sides, with a thickness of approximately 100 nm that was deposited using a Quorom Q150R ES sputtering.

3. RESULTS AND DISCUSSION

Films of the $BaTiO_3$/PA mixture were produced under varying process conditions, specifically in terms of laser scanning speed and applied power. The scanning speeds employed were 1.0, 1.2, and 1.5 mm/s, while the applied nominal laser power values were 10.2, 12.6, and 15.2 W. In total, 9 batches of samples were fabricated, each consisting of 4 films with an area of ~12 × 12 mm. A representative film from each batch is shown in Figure **2**, and the average thickness measurements of the films are summarized in Table **1**. The surface of the green film appeared visually smooth. It was also found that increasing the layer thickness led to an increase in surface roughness.

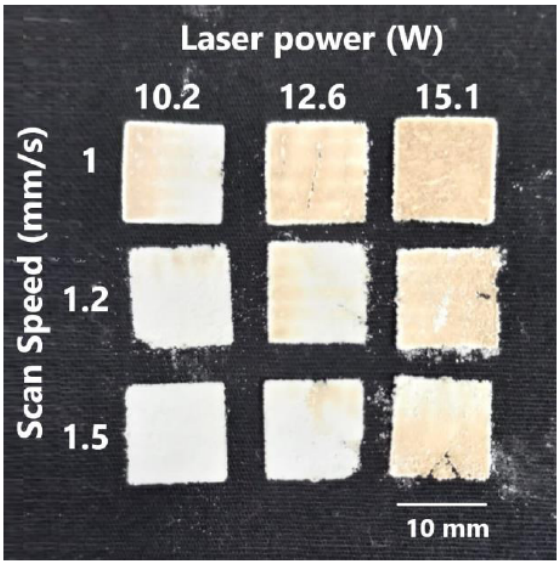

Figure 2: Optical image of the $BaTiO_3$/PA films obtained after ISLS using different nominal laser power (P) and scanning speeds (S).

Based on the results obtained, it can be noted that for all the values of scanning speed and power used, it has been possible to obtain thick films with enough mechanical strength to be manipulated. The thickness of the film, as expected, is dependent on the scanning speed and laser power. For slow scanning speeds and high power, the green thick film has a greater thickness. This occurs because in this condition, the laser provides energy over an extended duration at each point on the scanned line, elevating the surface

Table 1: Data of the Average Thickness (in mm ± 0.01) of the $BaTiO_3$ Green Thick Films were Obtained after the Laser Sintering Process, for each Laser Scanning Speed and Laser Nominal Power Used

Laser Power (W) / Scan Speed (mm/s)	10.2	12.6	15.2
1.0	0.61	0.63	0.67
1.2	0.45	0.49	0.60
1.5	0.30	0.38	0.50

temperature and facilitating heat conduction to a deeper depth. This process melts more polyamide beneath the surface, increasing the thickness of the film. Conversely, when the laser line scan speed is faster, the polyamide inside the powder bed does not have enough time to melt, resulting in thinner films. Figure **3** and Table **1** illustrate the effect of the laser power and scan speed on the thickness of the films after ISLS.

The X-ray diffraction measurement for the sintered $BaTiO_3$ film is shown in Figure **4**. The peaks could be identified as the tetragonal phase of $BaTiO_3$ since the powder diffraction peaks were in good agreement with the standard diffraction peaks, and no detectable intensities corresponding to PA12 or its residues. The XRD patterns revealed ten diffraction peaks, attributed to the perovskite $BaTiO_3$ phase. Notably, the split peak at 2θ ~ 45° was identified as the (002) and (200) reflections of tetragonal $BaTiO_3$ (inset of Figure **4**), confirming that the BT particles exhibit a well-defined tetragonal phase [11, 12].

The Raman spectrum of the $BaTiO_3$ film is presented in Figure **5**. The peaks observed at 264 cm^{-1}, 305 cm^{-1}, 518 cm^{-1}, and 716 cm^{-1} correspond to the Raman shifts characteristic of barium titanate [11]. The intense peaks at 264 cm^{-1} and 305 cm^{-1} are attributed to the vibrations of the TiO_6 group, while the peak at 518 cm^{-1} is associated with vibrations caused by the displacement of oxygen atoms. The Raman active peaks identified are consistent with the characteristic peaks of $BaTiO_3$ reported in the literature. Furthermore, the presence of peaks at 305 cm^{-1} and 716 cm^{-1}

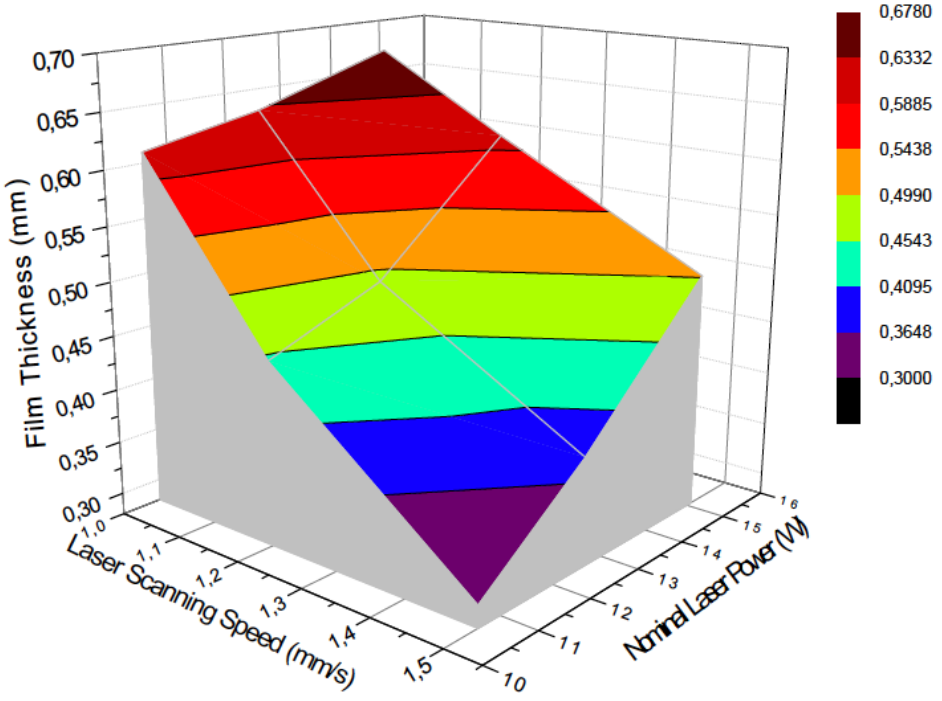

Figure 3: Measurements of the effect of applied laser power and scanning speed on the thickness of the green $BaTiO_3$ thick film.

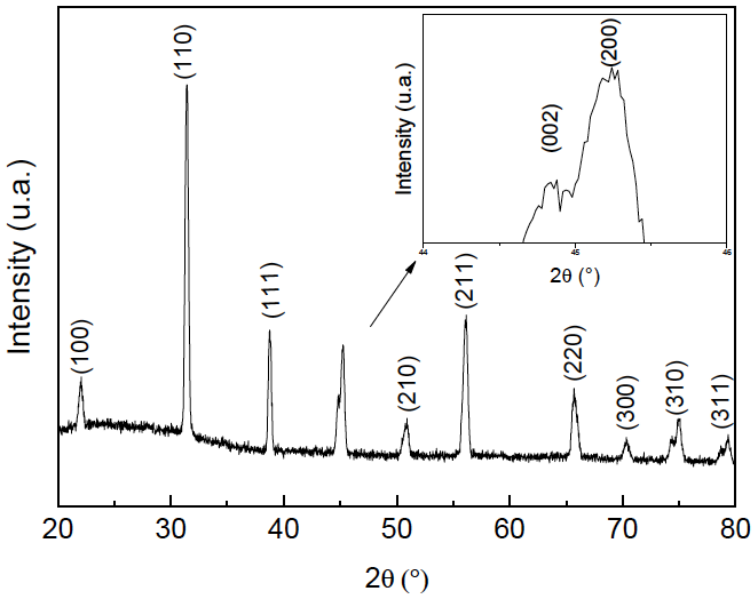

Figure 4: Diffraction pattern results of the $BaTiO_3$ film, sintered at 1200°C for 3 hours.

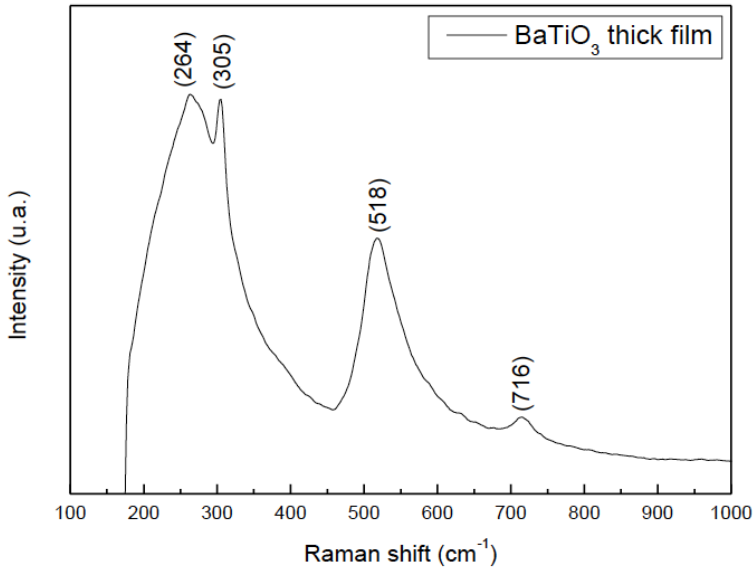

Figure 5: Raman spectrum for the sintered $BaTiO_3$ thick film, indicating the active Raman shifts observed.

confirms the presence of the tetragonal phase of $BaTiO_3$ [11].

The morphology of the $BaTiO_3$ films is shown in Figure **6**. The microstructures reveal the presence of grains of varying sizes with well-defined contours, indicating the polycrystalline nature of the material. The sample exhibits a porous structure characterized by a uniform distribution of grains along with the presence of some agglomerates.

The MIP data is shown in Figure **7**, as the cumulative volume curve and the fitting using a double Boltzmann equation. The pore volume and size distribution indicate two distinct intrusion patterns within the pore size range of 0.2 to 10 µm, suggesting a bimodal pore distribution. The first distribution spans from 0.1 to 4 µm, while the second is observed in the 7 to 9 µm range. The total pore volume measured was 0.142 cm³/g, and the sample's porosity, calculated from the cumulative pore volume, was approximately 16%. Additionally, for pores larger than 20 µm, no significant mercury intrusion was detected, indicating that this is the maximum diameter present in the interconnected porous network.

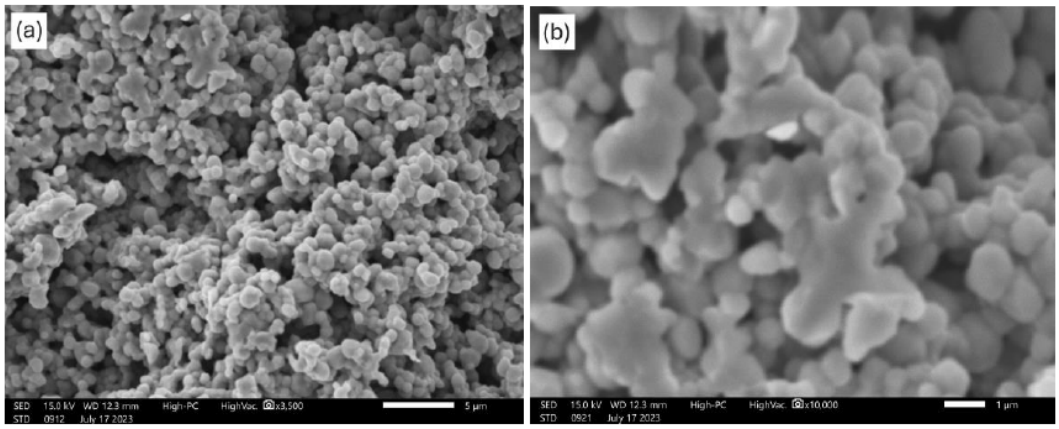

Figure 6: Fracture surface micrographs of the $BaTiO_3$ film, sintered at 1200°C for 3 hours, captured at different magnifications to highlight the film's morphology. (**a**) The porous nature of the film and (**b**) higher magnification of a region with more sintered structure.

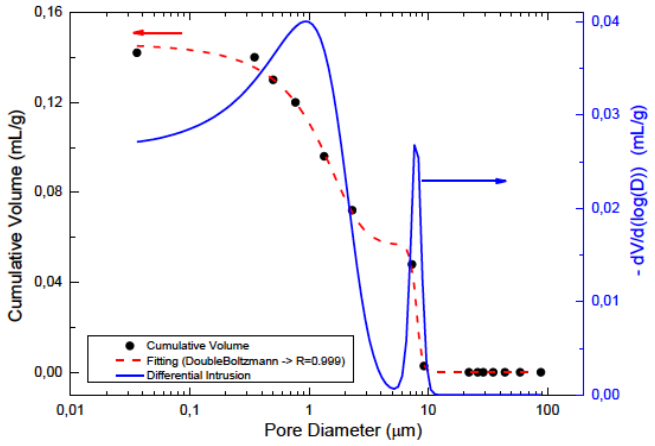

Figure 7: Fitting to the experimental curve of the cumulative pore volume measured by MIP in the $BaTiO_3$ film.

$BaTiO_3$ was the first ceramic material with ferroelectric properties discovered and synthesized in the laboratory in the 1940s [13]. However, to this day there is still some controversy in the literature about experimental results concerning the PTCR effect in pure barium titanate ceramics [14-18] or even the origin of the semiconductivity in this compound [18].

To determine whether the prepared thick films exhibited the PTCR effect, impedance spectroscopy was conducted. Figure **8** illustrates the variation of the effective electrical resistivity, considered as the real impedance multiplied by the geometrical factor (electrode area divided by the thickness of the film) from room temperature of 25°C to 300°C, with the error bars representing the fitting uncertainty. The results indicate an increase in the total effective resistivity of the material as the temperature rises. The onset temperature of the PTCR effect was observed to be slightly below the Curie temperature of $BaTiO_3$, which is approximately 120°C. It was observed that the room temperature effective resistivity presents lower values with respect to typical pure $BaTiO_3$ ceramics, which are considered insulators with average room temperature resistivity up to 10^{12} ohm.cm. On the other hand, the peak of the effective resistivity achieved a value of approximately $7x10^7$ ohm.cm, which is coherent with a thermistor material, and also presents a significant rate of decrease, achieving values of the same order as the room temperature resistivity.

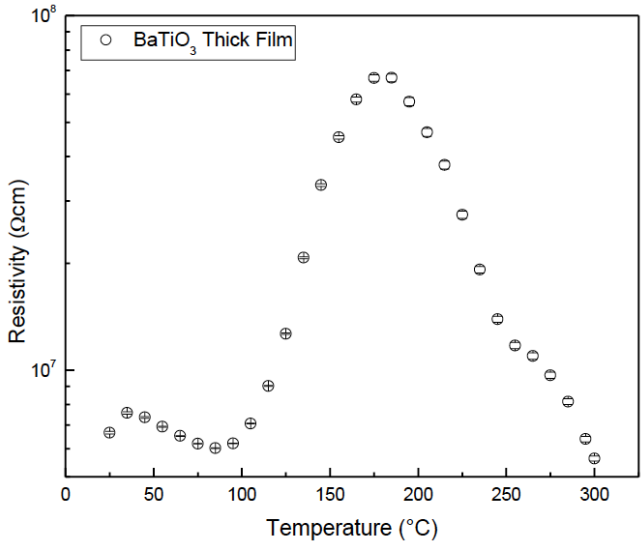

Figure 8: AC Resistivity versus temperature for a $BaTiO_3$ film.

One possible hypothesis to explain the PTCR effect on the thick films produced, which is currently under investigation, might be related to the oxygen adsorption and oxygen vacancies. During the sintering process of

the thick films, the PA12 degradation can produce a carbon coating on the grains and their boundaries that might create oxygen deficiencies in the barium titanate during heating (especially at the grain boundaries), as shown in equation 1. These possible oxygen vacancies might be the origin for the semiconducting state in the barium titanate.

$$C_{(solid)} + O_o^x \rightarrow CO_{(gas)} + V_o^{\bullet\bullet} + 2e^{'} \quad (1)$$

Once those defects are created, it has been reported that it is very difficult to achieve complete reoxidation of barium titanate [19].

In this way, it is possible that the origin of the observed PTCR effect, on the prepared thick films, lies basically in a two-fold process. The first is related to the porosity (allowing a larger surface area for oxygen adsorption on the grains and grain boundaries) and the second may be due to the oxygen vacancies created by the reaction with the carbon residues due to the PA12 degradation during the sintering process.

4. CONCLUSION

This study demonstrates the feasibility of using an adapted indirect selective laser sintering (ISLS) technique to produce porous, free-standing thick films of ferroelectric $BaTiO_3$. The process enabled the rapid forming of the film, whose thickness can be controlled by adjusting the pair of variables, laser scanning speed and laser power. The measurements confirmed the tetragonal $BaTiO_3$ phases and a bimodal porosity. Evidence of PTCR effect was also detected, the origin of which is still under investigation and may be related to the film porosity and the possible oxygen vacancies generated during the heating process due to the PA12 degradation. These findings highlight that this method has the potential to efficiently fabricate functional ferroelectric thick films for a variety of technological applications.

ACKNOWLEDGMENTS

This study was partially financed by the Coordination and Improvement of Higher Level or Education Personnel (Capes), Finance Code 001. The authors would also like to thank the Center for Research, Technology and Education in Vitreous Materials (CeRTEV), at the Federal University of São Carlos, for the general facilities and the São Paulo Research Foundation, FAPESP for the financial support (grants: #2013/07793-6, #2013/17071-8 and #2019/27628-6). Mendes, F.B. would like to thank the Conselho Nacional de Desenvolvimento Científico e Tecnológico (CNPq) (Brazil) under grant #141261/2024-2.

CONFLICTS OF INTEREST

The authors declare that there are no conflicts of interest related to the content of this article.

REFERENCES

[1] Provo JL. History of very thick film and bulk sample group IIIB, IVB, VB, and rare earth materials for various vacuum applications. Journal of Vacuum Science & Technology A: Vacuum, Surfaces, and Films. 2018 Jul 1; 36(4). https://doi.org/10.1116/1.5038880

[2] Faraday M. X. The Bakerian Lecture. -Experimental relations of gold (and other metals) to light. Philos Trans R Soc Lond. 1857; 147: 145-81. https://doi.org/10.1098/rstl.1857.0011

[3] Dunce M, Plyushch A, Birks E, Svirskas Š, Banys J, Jankauskas P, Bikse L, Atvars A, Freimanis O, Leimane M, Bundulis A. Free-standing 0.9Na0.5Bi0.5TiO3-0.1Sr0.7Bi0.2TiO3 thick films produced by water-based tape-casting method. Journal of the American Ceramic Society. 2024 Oct 1; 107(10): 6532-43. https://doi.org/10.1111/jace.19944

[4] Gao J, Ma W, Yang Y, Guo J, Zhao H, Ma M. The free-standing multilayer thick films of 0.7Pb(Zr0.46Ti0.54)O3-0.1Pb(Zn1/3Nb2/3)O3-0.2Pb(Ni1/3Nb2/3)O3 with low co-fired temperature. Journal of Materials Science: Materials in Electronics. 2018 Jul 1; 29(14): 11664-71. https://doi.org/10.1007/s10854-018-9263-1

[5] Maier JG, Fuggerer T, Urushihara D, Martin A, Khansur NH, Kakimoto KI, Webber KG. The Impact of Grain Growth on the Functional Properties in Room-Temperature Powder Aerosol Deposited Free-Standing (Ba,Ca)(Zr,Ti)O3 Thick Films. Crystals (Basel). 2024 Apr 1; 14(4): 296. https://doi.org/10.3390/cryst14040296

[6] Lucat C, Ginet P, Ménil F. New Sacrificial Layer-Based Screen-Printing Process for Free-Standing Thick-Films Applied to MEMS. Journal of Microelectronics and Electronic Packaging. 2007; 4(3): 86-92. https://doi.org/10.4071/1551-4897-4.3.86

[7] Lee KJ, Cho WS. Microstructure and PTCR characteristics of porous BaTiO3-based ceramics prepared by adding activated carbon. Metals and Materials International. 2012 Oct 10; 18(5): 887-93. https://doi.org/10.1007/s12540-012-5022-7

[8] Andreeta MRB, Mendes FB, Bonacin RO. Selective laser sintering process for the fabrication of free-standing films, the free-standing films thus obtained, and their uses. INPI: BR1020230268, 2023.

[9] Grossin D, Montón A, Navarrete-Segado P, Özmen E, Urruth G, Maury F, Maury D, Frances C, Tourbin M, Lenormand P, Bertrand G. A review of additive manufacturing of ceramics by powder bed selective laser processing (sintering / melting): Calcium phosphate, silicon carbide, zirconia, alumina, and their composites. Open Ceramics. 2021 Mar; 5: 100073. https://doi.org/10.1016/j.oceram.2021.100073

[10] Mendes FB. Study of the process for obtaining free-standing porous thick films through selective laser sintering (in Portuguese). [São Carlos, SP - Brazil]: Federal University of São Carlos; 2023.

[11] Sun Q, Gu Q, Zhu K, Jin R, Liu J, Wang J, Qiu J. Crystalline Structure, Defect Chemistry and Room Temperature Colossal Permittivity of Nd-doped Barium Titanate. Sci Rep. 2017 Feb 13; 7(1): 42274. https://doi.org/10.1038/srep42274

[12] Isohama Y, Nakajima N, Maruyama H, Tezuka Y, Iwazumi T. Tetragonal-cubic phase transition in BaTiO3 probed by resonant X-ray emission spectroscopy. J Electron Spectros Relat Phenomena. 2011 Apr 1; 184(3-6): 207-9. https://doi.org/10.1016/j.elspec.2010.12.023

[13] Moulson AJ, Herbert JM. Electroceramics. Wiley; 2003. https://doi.org/10.1002/0470867965

[14] Aga ZBH, Ramanan SR. Electrical and structural characterization of PTCR pure BaTiO3 nanopowders synthesized by sol-gel emulsion technique. J Electroceram. 2012 May 12; 28(2-3): 109-17. https://doi.org/10.1007/s10832-012-9690-y

[15] Alles AB, Amarakoon VRW, Burdick VL. Positive Temperature Coefficient of Resistivity Effect in Undoped, Atmospherically Reduced Barium Titanate. Journal of the American Ceramic Society. 1989 Jan 8; 72(1): 148-51. https://doi.org/10.1111/j.1151-2916.1989.tb05970.x

[16] Cook WR. Comment on "Positive Temperature Coefficient of Resistivity Effect in Undoped Atmospherically Reduced Barium Titanate." Journal of the American Ceramic Society. 1991 Jul 8; 74(7): 1749-1749. https://doi.org/10.1111/j.1151-2916.1991.tb07180.x

[17] Alles AB, Amarakoon VRW, Burdick VL. Reply to "Comment on 'Positive Temperature Coefficient of Resistivity Effect in Undoped Atmospherically Reduced Barium Titanate.'" Journal of the American Ceramic Society. 1991 Jul 8; 74(7): 1750-1750. https://doi.org/10.1111/j.1151-2916.1991.tb07181.x

[18] Murakami T. The PTCR Effect in BaTiO3 Single Crystals. Jpn J Appl Phys. 1966 May 1; 5(5): 450. https://doi.org/10.1143/JJAP.5.450

[19] Beltrán H, Cordoncillo E, Escribano P, Sinclair DC, West AR. Oxygen loss, semiconductivity, and positive temperature coefficient of resistance behavior in undoped cation-stoichiometric BaTiO3 ceramics. J Appl Phys. 2005 Nov 1; 98(9). https://doi.org/10.1063/1.2089158

Received on 28-11-2024 Accepted on 24-12-2024 Published on 30-12-2024

https://doi.org/10.31875/2410-4701.2024.11.12